CSIRO PUBLISHING

RESEARCH FRONT

Environ. Chem. **2015**, *12*, 74–84
http://dx.doi.org/10.1071/EN14065

Research Paper

Adsorption of novel insensitive munitions compounds at clay mineral and metal oxide surfaces

Billy R. Linker,[A] *Raju Khatiwada,*[A] *Nico Perdrial,*[A,B] *Leif Abrell,*[A,C] *Reyes Sierra-Alvarez,*[D] *James A. Field*[D] *and Jon Chorover*[A,C,E]

[A]Department of Soil, Water and Environmental Science, University of Arizona, PO Box 210038, Tucson, AZ 85721-0038, USA.
[B]Department of Geology, University of Vermont, 213 Delehanty Hall, Burlington, VT, 05405, USA.
[C]Arizona Laboratory for Emerging Contaminants, Department of Soil, Water and Environmental Science, University of Arizona, PO Box 210038, Tucson, AZ 85721-0038, USA.
[D]Department of Chemical and Environmental Engineering, University of Arizona, PO Box 210020, Tucson, AZ 85721-0020, USA.
[E]Corresponding author. Email: chorover@email.arizona.edu

Environmental context. Insensitive munitions compounds are increasingly used in the manufacture of military energetic materials because of their lower unintentional explosion risk during transport and handling. The current study was designed to better resolve the environmental chemistry of two of these insensitive munitions compounds. In particular, we investigated the solid–solution partitioning that occurs when aqueous solutions containing dissolved unexploded ordinances come into contact with soil mineral media.

Abstract. Insensitive munitions compounds (IMCs) are increasingly used for military energetic materials, yet their environmental fate is poorly understood. Prior work has shown that the nitroaromatic 2,4-dinitroanisole (DNAN) and the heterocyclic nitrogen compound 3-nitro-1,2,4-triazole-5-one (NTO), both newly introduced IMCs, can undergo microbially mediated reduction under anoxic conditions to form 2-methoxy-5-nitroaniline (MENA) and 3-amino-1,2,4, triazole-5-one (ATO) respectively. In the present work, DNAN, MENA, NTO and ATO were subjected to batch adsorption–desorption experiments with specimen soil mineral adsorbents that included montmorillonite, birnessite and goethite. DNAN and MENA exhibited high affinity, linear adsorption to montmorillonite, with enhanced surface excess at a given aqueous equilibrium concentration for K^+-saturated relative to Na^+-saturated forms, but negligible adsorption to the metal oxides. Powder X-ray diffraction data and surface occupancy calculations indicate interlayer intrusion by DNAN and MENA and adsorption at siloxane sites. Conversely, NTO and ATO exhibited low sorptive affinity and apparent anion exclusion upon reaction with the negatively charged layer silicate clays. However, both of the N-heterocycles showed positive adsorption affinities for goethite (K_d values of 11.1 and 3.1, and HI values of 1.8 and 0.50 respectively), consistent with anion adsorption to the positively charged goethite surface. Both ATO and MENA were subjected to apparent oxidative, abiotic chemical transformation during reaction with birnessite. The results indicate that the IMCs studied will exhibit adsorptive retardation – and their biodegradation products may undergo further abiotic transformation – upon reaction at soil mineral surfaces.

Received 31 March 2014, accepted 22 September 2014, published online 7 January 2015

Introduction

Manufacturing, handling and transportation of military energetic (i.e. 'explosive') material represent a hazardous enterprise, and insensitive munitions compounds (IMCs) are being developed to mitigate these hazards. IMCs are chemically energetic compounds that are more resistant than traditional energetic compounds to unintended stimuli including shock and high temperatures.[1] Traditional energetics, such as 2,4,6-trinitrotoluene (TNT), have long been used for military applications. However, as military operations look to reduce explosive hazards, the use of TNT and less stable compounds are seeing a decrease in use in favour of more stable chemical alternatives. An increased production and use of IMCs could lead to a higher prevalence in soils and ground water around manufacturing facilities and military testing ranges.

IMCs include both nitroaromatic compounds (NACs) and N-heterocyclic compounds (NHCs). NACs are commonly used as energetic compounds, pesticides and dye precursors.[2] Environmental concerns derive from the fact that many NACs are toxic.[3] Certain NACs have mutagenic characteristics and have been placed on the USA Environmental Protection Agency's list of priority pollutants.[4,5] NHCs, including energetic compounds, can also be toxic.[6] Given their potential for adverse environmental effects, and that the behaviour of these IMCs in environmental systems is presently unknown, a detailed investigation is warranted.

Two IMCs of particular interest for USA Department of Defence deployment include 2,4-dinitroanisole (DNAN) and 3-nitro-1,2,4-triazole-5-one (NTO).[1,7] Both of these compounds have been shown to undergo microbially mediated reductive transformation under anoxic conditions, as commonly occurs within bio-active soil aggregates subjected to precipitation events. Prior experiments conducted in our research group indicate that DNAN, the nitroaromatic IMC, undergoes biotransformation under anoxic conditions to form 2-methoxy-5-nitroaniline (MENA).[8] Likewise, previous work has shown that NTO undergoes reductive biotransformation to 3-amino-1,2,4,triazole-5-one (ATO).[9] Therefore, an assessment of environmental partitioning of DNAN and NTO should also include their (bio)transformation products MENA and ATO in order to predict more comprehensively the environmental fate of these IMCs.

Organic matter is commonly assumed to dominate the sorptive retention of hydrophobic organic contaminants in soils, but the affinity of organic compounds for mineral surfaces can also be very high, particularly for compounds comprising polar functional groups, such that significant underestimates of contaminant retention may result from consideration of organic matter alone.[10] The siloxane surfaces of layer silicate clays, such as smectite, have been shown to be effective sorbents for NACs.[2,10,11] The type of exchangeable interlayer cation (e.g. K^+ *v.* Na^+) has also been shown to affect the uptake of NACs by layer silicate clays: cations of lower hydration energy (e.g. K^+ relative to Na^+) may increase adsorptive affinity,[2,10,12] highlighting the potential for significant effects on organic sorptive retention of reasonably small changes in mineral surface chemistry. In prior work, silicate clays have been shown to exhibit pH-dependent affinity for NHCs such as acridine[13] or quinoline,[14] although with significant modulating effects of exchangeable cation or adsorbed natural organic matter.

Metal (oxyhydr)oxides are ubiquitous soil constituents that can also affect contaminant retention at their variably charged hydroxylated surfaces. Iron (oxyhydr)oxides such as goethite and lepidocrocite present polar, pH-dependent charged surfaces that can affect electrostatic or covalent bonding of aromatic compounds comprising charged or polar functionalities.[15,16] Whereas manganese(III, IV) oxides also represent a significant fraction of a reactive interface in soils, they are among the strongest oxidants outside of molecular oxygen present in soils.[17] For example, the Mn^{IV} oxide birnessite was observed to oxidise aromatic amines such as toxic *p*-methoxyaniline and α-naphthylamine[18] and converted catechol (dihydroxybenzene) into polymerised products and CO_2.[19] The oxidation and subsequent polymerisation of aromatic amines into larger or smaller molecular weight compounds is a potential mechanism for reducing their mobility in soils.

Despite the fact that layer silicate clays and metal oxides dominate the reactive interfacial area of soil systems,[20] the adsorption–desorption behaviour of new IMCs at such surfaces remains unknown. This leaves a significant gap in our ability to develop mechanistic models of the transport and fate of these contaminants in aqueous mineral soil systems, which are the principal recipients of unexploded IMC residues. An improved understanding of IMC environmental fate requires a knowledge of how these contaminants react at representative mineral surfaces, including the charged siloxane surfaces of layer silicate clays and the hydroxylated surfaces of metal (oxy)hydroxides. Therefore, the objectives of this study were to (1) determine the adsorption affinity of the IMCs DNAN and NTO, as well as their microbial reduction products MENA and ATO, in abiotic aqueous suspensions of smectite, goethite and birnessite and (2) assess whether any abiotic transformation reactions may ensue as a result of sorbent–sorbate interaction.

Materials and methods

The present study involved quantification of adsorption and desorption of DNAN, MENA, NTO and ATO on representative soil mineral sorbents including a 2 : 1 layer silicate (montmorillonite), an iron oxyhydroxide (goethite) and a manganese oxide (acid birnessite). These specimen mineral constituents were chosen because of their ubiquitous occurrence in soils worldwide, and for their representative range of surface chemical properties. The study also investigated the effects of saturated interlayer cation type (K^+, Na^+) on IMC adsorption.

Mineral synthesis and clay preparation

Wyoming montmorillonite (SWy-2) was acquired from the Source Clay Minerals Repository, University of Missouri. Forty grams of clay were added to 1 kg of ultrapure (18 mΩ cm^{-1}) water and dispersed for size fractionation by adjustment of the suspension pH value to 8.0 through the addition of 0.01 M NaOH. The <2-μm size fraction was collected by extraction of the supernatant suspension following centrifugation in 250-mL polypropylene copolymer (PPCO) bottles for 5 min at 152*g* at 25 °C. The suspension was then flocculated by addition of 0.001 M HCl in 1.0 M NaCl for 20 min, followed by centrifugation for 10 min at 7500 rpm. This process was repeated until the pH value of the supernatant was equivalent to the pH value of the wash solution, approximately pH 3. The clays were then dispersed in 0.01 M NaCl for 20 min, followed by centrifugation for 10 min at 8540*g*, and the process repeated until the pH value of the supernatant reached pH 5.5. The clays, suspended in 0.01 M NaCl, were then stored in a refrigerator at 2.8 °C. The same protocol was followed for K^+ saturation of the montmorillonite. The final solid concentration of montmorillonite was 29.6 and 24.2 g L^{-1} for Na^+- and K^+-saturated forms.

Goethite was synthesised by addition of 0.2 L of 2.5 M KOH to 50 g of $Fe(NO_3)_3 \cdot 9H_2O$ (VWR Scientific, Denver, CO) in 0.825 L of 18 mΩ cm^{-1} water and heated at 60 °C for 24 h. Excess liquid was discarded and the remaining solids were distributed evenly into four 250-mL PPCO centrifuge bottles. Solids were washed with 0.1 mM HCl solution until the supernatant reached pH 5 and residual nitrate was removed.[21]

Birnessite was synthesised by addition of 0.0664 L of 12 M HCl to 1 kg of boiling 0.4 M potassium permanganate solution (VWR Scientific). The precipitate was collected, mixed with 1 mM HCl for 30 min, and divided into ten 50-mL Teflon centrifuge tubes. Tubes were centrifuged at 41 500*g* for 10 min. This process was repeated until the supernatant reached pH 4, and then the solids were freeze-dried.[22]

Successful birnessite and goethite mineral synthesis was confirmed by synchrotron radiation X-ray diffraction (SR-XRD) analysis at the Stanford Synchrotron Radiation Lightsource (SSRL) on beam line 11-3 operating at ~12 735 eV in transmission mode, using a 345-mm radius Mar detector with a resolution of 100-μm pixels. For SR-XRD analysis, ~10 mg of material were packed between two layers of Scotch Magic matte finish tape (St Paul, MN, USA) to obtain a homogeneous thin layer sample. After calibration of the detector using finely ground LaB6 crystals, three scans were collected for each sample and added. Data were reduced using the Area Diffraction Machine software

Table 1. Mineral adsorbents and pertinent characteristics

Mineral	Chemical formula	Specific surface area ($m^2\ g^{-1}$)	pH_{pznc} (point of zero net charge)
Montmorillonite	$(Na_{0.32}\ Ca_{0.12}\ K_{0.05})[Al_{3.01}\ Fe^{III}_{0.41}\ Mn_{0.01}\ Mg_{.54}Ti_{0.02}]$ $[Si_{7.98}\ Al_{0.02}]O_{20}(OH)_4$	596[23]	3.4[37]
Goethite	α-FeO(OH)	50.1 ± 0.2[23]	7.5[33]
Birnessite	$(Na_{0.3}Ca_{0.1}K_{0.1})(Mn^{4+},Mn^{3+})_2O_4 \cdot 1.5H_2O)$	83.8 ± 0.7[23]	1.9[33]

(by J. Lande, S. Webb and A. Mehta) with a mask covering the beamstop. The mineral specific surface areas (SSA) measured previously by N_2-Brunauer–Emmett–Teller (BET) for specimen minerals prepared by the same methods[23] are reported in Table 1. The ethylene glycol monoethyl ether adsorption method was used to measure the total (including internal) specific surface area of montmorillonite (596 $m^2\ g^{-1}$).

Insensitive munitions compounds and biotransformation products

The compounds used in adsorption experiments were either purchased or synthesised. The 2,4-dinitroanisole (DNAN; CAS # 119-27-7, 98 % purity) was purchased from Alfa Aesar (Ward Hill, MA). The 2-methoxy-5-nitroaniline (MENA; CAS # 99-59-2, 98 % purity) was purchased from Sigma–Aldrich (St Louis, MO). The 3-nitro-1,2,4-triazol-5-one (NTO; CAS # 932-64-9, >95 % purity) was purchased from Interchim (Montlucon, France). The 3-amino-1,2,4-triazol-5-one (ATO) was synthesised by adapting the palladium on carbon (Pd/C) reduction method according to LeCampion et al.[24] Briefly, NTO, Pd/C and methanol were combined in darkness in a serum bottle, the headspace flushed with helium gas for 5 min, and then pressurised to ~10 psi with H_2 gas. The bottle was placed on a shaker table, and fresh H_2 gas added until the reaction ceased to consume H_2. The contents were then filtered through a 0.22-μm polyethersulfone filter (EMD Millipore, Darmstadt, Germany) to remove any remaining solid catalyst and a rotovap used to remove the excess methanol. The contents were then dried to a solid under a He or N_2 gas stream. The resultant ATO, a white or slightly yellow powder, was stored in the dark in a refrigerator. Physicochemical information for the IMCs DNAN and NTO, as well as ATO and MENA, are provided in Table 2.

Batch adsorption–desorption method

All solutions were prepared and experiments conducted in darkness by encasing IMC stock containers and reaction vessels in aluminium foil in order to avoid potential photochemical degradation reactions.[25,26] IMCs were dissolved in 0.01 M NaCl or 0.01 M KCl solutions at maximum solution phase concentrations of 1.0 mmol kg^{-1} (below aqueous solubility). The IMC solution pH was adjusted to 7 with the addition of 0.01 M NaOH or 0.01 M HCl. Perfluoroalkoxy (PFA) microcentrifuge tubes (Savillex Corporation, Eden Prairie, MN) were used as reaction vessels. Approximately 0.4 mL of clay suspension was added to the reaction vessels, resulting in solid concentrations of 9.1 and 7.5 g L^{-1} for Na^+-saturated and K^+-saturated montmorillonite respectively. IMC solutions were diluted with 0.01 M NaCl or 0.01 M KCl to achieve known initial concentrations.

Birnessite and goethite were added to reaction vessels in solid form. These suspensions were prepared with a solid concentration of ~15 g L^{-1}, but all masses (solids, liquids, vessels) were measured precisely for later adsorption calculations. For birnessite and goethite experiments, IMC solutions were diluted with 0.01 M NaCl (KCl was not used in the metal oxide studies) to achieve known initial concentrations. Reaction vessels were mixed at 10 rpm on a rotational (end-over-end) mixer for 3 h in the dark at room temperature. Following mixing, solids were separated by centrifugation at 15 300*g* for 10 min using an Eppendorf 5417C bench top microcentrifuge. Method blanks were prepared using aliquots of IMC solutions without the addition of any solids or clay suspension to account for any loss of IMC as a result of vessel adsorption, and the equilibrated solution phase concentration values in the blanks were assumed equivalent to the 'initial' concentration for the adsorption experiments. The sorbed concentrations of IMCs were determined by the difference between aqueous initial and final equilibrium concentrations as measured by ultra-high performance liquid chromatography (Agilent 1290, Santa Clara, CA) with diode array detection (DAD) using:

$$q_{ads} = \frac{C_i - C_e}{M_{SLD}} M_{SLN} \quad (1)$$

where q_{ads} is the mass of sorbed IMC per unit mass of solid sorbent (mmol $kg^{-1}{}_{SLD}$) at equilibrium after the adsorption step, C_i and C_e are the initial and equilibrium IMC concentrations (mmol $kg^{-1}{}_{SLN}$), M_{SLD} is the total mass of solid (kg) and M_{SLN} is the total mass of solution (kg).

Following the adsorption step, excess solution was decanted from vessels. Sedimented pellets were then suspended in the appropriate background electrolyte solution (0.01 M NaCl or 0.01 M KCl). Vessels were again mixed using the conditions above, centrifuged, decanted and the supernatant solutions analysed to determine the extent of desorption. Adsorbed IMC concentrations after the desorption step were determined by:

$$q_{des} = q_{ads} - \left(\left(\frac{C_{e,des} M_{SLN}}{M_{SLD}}\right) - \left(\frac{C_{e,ads} M_{ENT}}{M_{SLD}}\right)\right) \quad (2)$$

where q_{des} is the mass of sorbed IMC per unit mass of solid sorbent (mmol $kg^{-1}{}_{SLD}$) at equilibrium after the desorption step, $C_{e,des}$ and $C_{e,ads}$ are the measured equilibrium IMC concentrations in solution (mmol $kg^{-1}{}_{SLN}$) after the desorption and adsorption steps respectively, and M_{ENT} is the mass of entrained solution remaining in the reaction vessel after decanting the supernatant solution (kg). Solid–solution partition coefficients (K_d) were calculated for linear isotherms. The K_d values were calculated by:

$$K_d = \frac{q_{ads}}{C_{e,ads}} \quad (3)$$

where q_{ads} is the mass of sorbed IMC per unit mass of solid sorbent (mmol $kg^{-1}{}_{SLD}$) and $C_{e,ads}$ is the solution phase IMC

Table 2. Insensitive munition compounds (IMCs) and physico-chemical parameters
N/A, not available; pK_a, acid dissociation constant; K_{OW}, octanol–water partition coefficient

IMC	Chemical name	Structure	Molecular weight	pK_a	Solubility (mg L^{-1})	log K_{OW}
DNAN	2,4-dinitroanisole	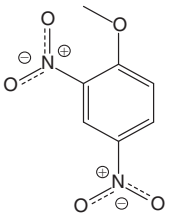	198.13	N/A	276 ± 2.5[7]	1.612[7]
MENA	2-methoxy-5-nitroaniline	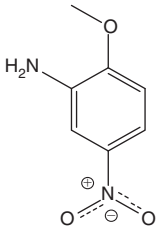	168.15	2.49[38]	115–3485[39] A	1.47[38]
NTO	3-nitro-1,2,4-triazole-5-one	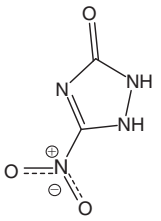	130.06	3.76[40]	12 800[1]	0.21 ± 0.4[39]
ATO	3-amino-1,2,4-triazole-5-one	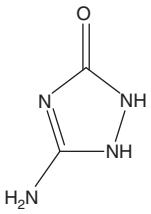	100.08	9.17	N/A	N/A

[A]Estimation from log K_{ow}.

concentration (mmol kg^{-1}_{SLN}), both measured at equilibrium. Hysteresis index (HI) values were also calculated for several isotherms. The HI is determined by comparing the surface excess values, q_{ads} and q_{des}, for the adsorption and desorption steps at a fixed value of aqueous analyte concentration.[27] The HI values were calculated by:

$$HI = \frac{q_{des} + q_{ads}}{q_{ads}} \quad (4)$$

NTO adsorption to birnessite and goethite was non-linear and the Freundlich isotherm equation provided a better fit to the data than a linear equation. The Freundlich fit was calculated using:

$$q_{ads} = KC^{n}_{e,ads} \quad (5)$$

where q_{ads} is the mass of sorbed of IMC per unit mass of solid sorbent (mmol kg^{-1}_{SLD}) at equilibrium, K is the Freundlich constant, $C_{e,ads}$ is the solution phase IMC concentration at equilibrium (mmol kg^{-1}_{SLN}), and n is the Freundlich exponent. K and n are both adjustable parameters calculated from a linearised log–log plot of surface excess v. aqueous analyte concentration.

Analytical methods

High performance liquid chromatography–diode array detection (HPLC-DAD)

Concentrations of DNAN, MENA, NTO and ATO in solution were analysed with an Agilent 1290 series (Santa Clara, CA) HPLC-DAD. Batch samples with DNAN and MENA (5-μL injection) were separated using an E2 Acclaim Explosives column (2.1 mm × 100 mm; 2.2 μM; Dionex, Salt Lake City, UT) at room temperature. Linear calibrations were run using known analyte concentrations from ~2 μM to 1 mM, of IMC, including blanks. The mobile phase (methanol–H_2O, 40 : 60, v/v) was introduced isocratically at a flow rate of 0.25 mL min^{-1} for 15 min and detector absorbance values were recorded at several wavelengths. Quantifications of DNAN and MENA were accomplished by peak integration of signals at 300 and 254 nm respectively, with retention times of 9.2 min for DNAN and 5.3 min for MENA. NTO and ATO samples (5-μL injection)

were separated using a Hypercarb column (4.6 × 100 mm; 5 μM; Thermo Fisher Scientific, Beverly, MA) at room temperature. The mobile phase, acetonitrile (ACN) and 0.1 % aqueous trifluoroacetic acid (TFA), was run at a flow rate of 1.0 mL min^{-1} for 20 min in a gradient as follows: 0 min with 100 % TFA and 0 % ACN; 11 min with 85 % TFA and 15 % ACN; 15 min with 50 % TFA and 50 % ACN and 19 min with 0 % TFA and 100 % ACN. Multi-wavelength absorbance was recorded, and detection of NTO and ATO was performed at 340 and 216.5 nm respectively, with retention times of 13.7 min for NTO and 7.4 min for ATO. The detection limits for DNAN, MENA, NTO and ATO were 4 (DNAN), 3 (MENA) and 1 mg L^{-1} (NTO, ATO).

Liquid chromatography quadrupole time of flight mass spectrometry (LC-QTOF-MS)

High resolution full scan mass spectra were obtained for MENA–birnessite samples using liquid chromatography introduction to a TripleTOF 5600 quadrupole TOF-MS (AB Sciex, Framingham, MA) equipped with an electrospray ionisation (ESI) source kept at 700 °C. The 10-μL samples were injected onto an Acclaim Explosives E1 column (4.6 × 250 mm; 5 μM; Dionex, Salt Lake City, UT) at 28 °C at a flow rate of 1000 μL min^{-1} in a 55 % aqueous acetonitrile (0.1 % formic acid) solvent system and separated by UHPLC-DAD using an UltiMate 3000 (Dionex, Sunnyvale, CA). Information dependent acquisition (IDA; 0.1-s cycle time, six triggered ions per cycle, mass range 35–1000) spectra were obtained in ESI positive ion mode with a capillary setting of 5.5 kV and declustering potential of 80 V. Samples were monitored at wavelengths of 210, 254 and 360 nm. High resolution full scan mass spectra for ATO–birnessite were obtained by infusion at a flow rate of 30 μL min^{-1} into the TOF-MS with ESI source kept at 440 °C. Spectra with a mass range of 35–1000 were obtained in ESI positive ion mode with a capillary setting of 5.5 kV and declustering potential of 80 V. *Analyst TF 1.6 with PeakView 1.2.0.3* and *Formula Finder 1.1.0.0* software applications were used to process spectroscopic data. Differential analysis of MENA–birnessite chromatograms was accomplished with *MetabolitePilot 1.5.0* (AB Sciex, Framingham, MA) under minimally predictive processing parameters.

Results

SR-XRD: synthesis products and clay characterisation

Goethite and birnessite mineral syntheses were verified by X-ray diffraction analysis at SSRL. Data for synthesis products were fitted to goethite and birnessite using a Rietveld simulation to the SR-XRD data. This synthesised manganese oxide appeared to have the closest fit to acid birnessite (in Area Diffraction Machine software).

Adsorption isotherms

Adsorption–desorption isotherm experiments were conducted at pH 7.0 at 10 mM ionic strength for the IMCs DNAN and NTO, as well as their respective degradation products, MENA and ATO. Four distinct mineral adsorbents were employed including (i) Na^+- and (ii) K^+-saturated montmorillonite, (iii) goethite and (iv) birnessite (Figs 1–4, Table 3). The isotherms show IMC surface excess (q) values calculated with Eqns 1–2 as a function of equilibrium adsorptive species concentration in solution. Distribution coefficient (K_d) values (Table 3) are determined from a linear fit to the slope of each isotherm.

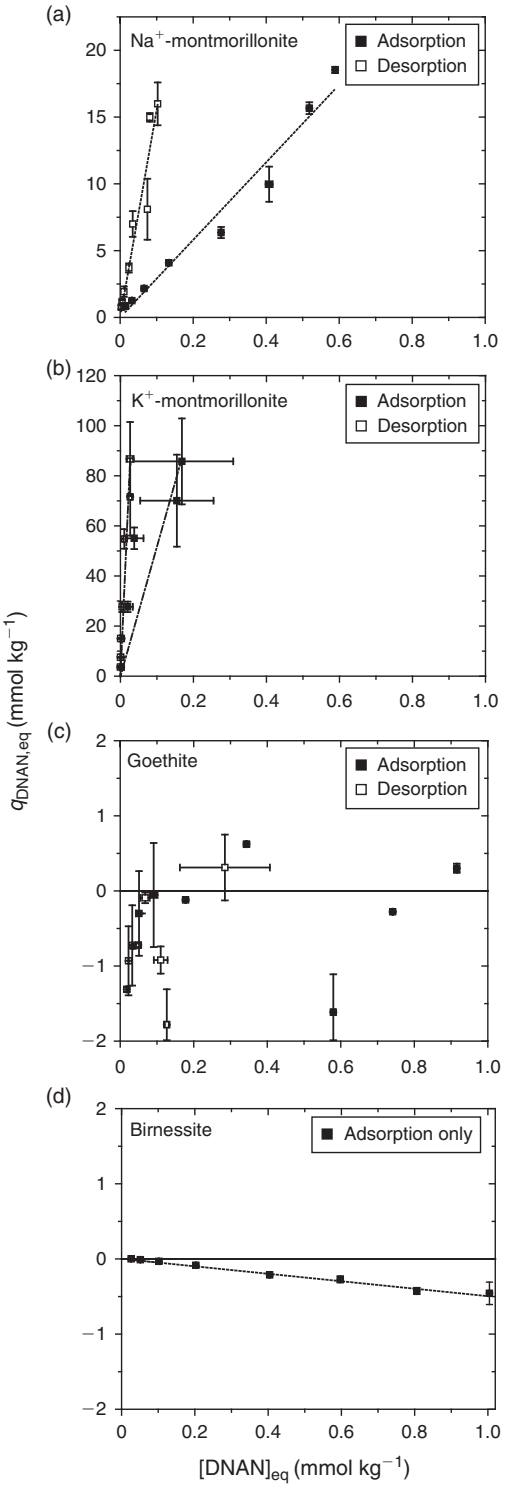

Fig. 1. Adsorption and desorption isotherms at pH 7.0 showing the uptake and release of 2,4-dinitroanisole (DNAN) at each mineral surface, where q represents the surface excess of adsorbate. Background electrolytes were 0.01 M NaCl for Na^+-montmorillonite, goethite, and birnessite and 0.01 M KCl for K^+-montmorillonite.

The data indicate that the NACs, DNAN (Fig. 1) and MENA (Fig. 2), have a positive affinity for montmorillonite but not for goethite. Comparing the Na^+- and K^+-montmorillonite isotherms in Fig. 2a demonstrates the large effect of exchangeable cation type on surface excess. For example, the K_d of DNAN is ~18 times higher for K^+- *v.* Na^+-saturated montmorillonite.

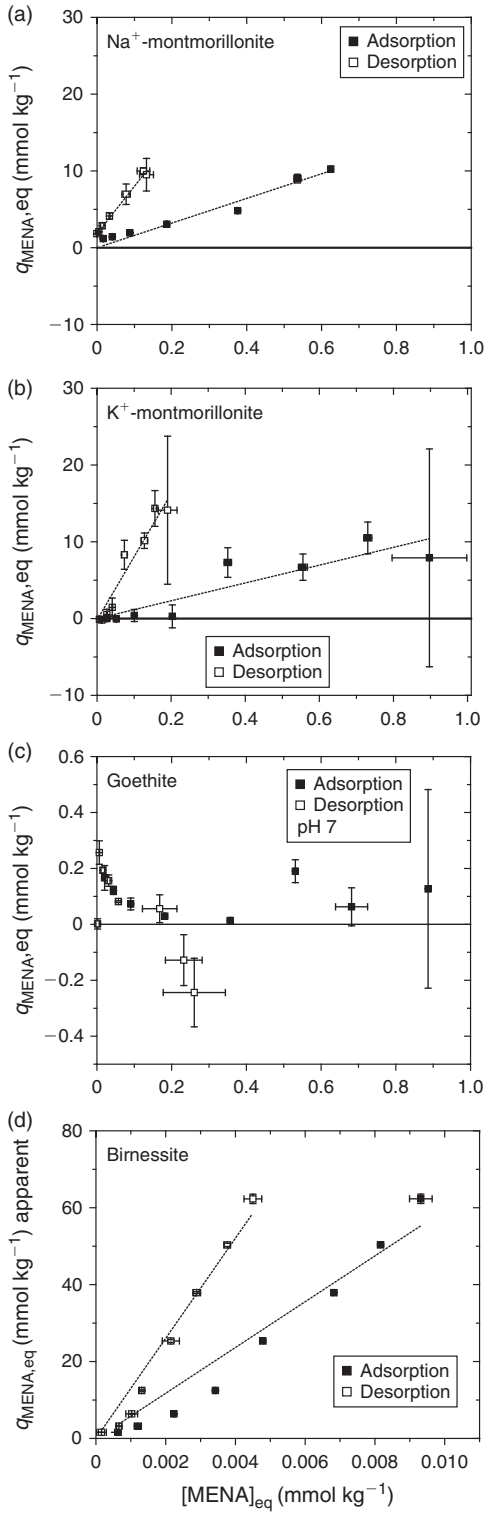

Fig. 2. Adsorption and desorption isotherms at pH 7.0 showing the uptake and release of 2-methoxy-5-nitroaniline (MENA) from each mineral surface, where q represents the surface excess of adsorbate (plot d is 'apparent' adsorption on the basis of loss from solution, later recognised to include oxidative transformation as discussed in the text). Background electrolytes were 0.01 M NaCl for Na^+-montmorillonite, goethite, and birnessite and 0.01 M KCl for K^+-montmorillonite.

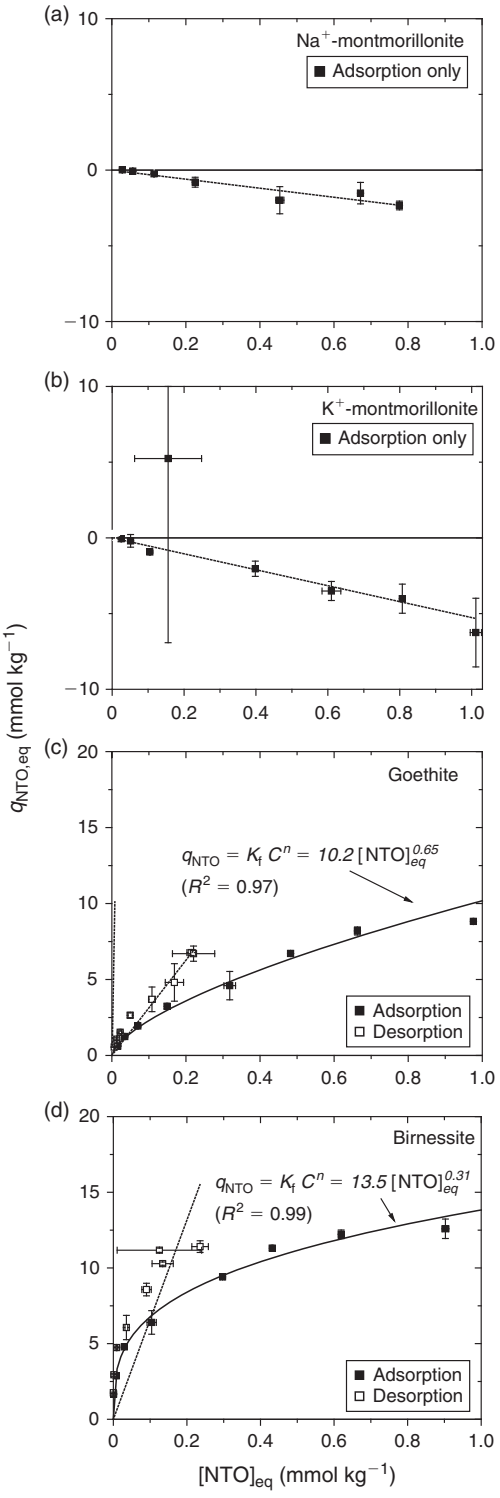

Fig. 3. Adsorption and desorption isotherms at pH 7.0 showing the uptake and release of 3-nitro-1,2,4-triazole-5-one (NTO) on each mineral surface, where q represents the surface excess of adsorbate. Background electrolytes were 0.01 M NaCl for Na^+-montmorillonite, goethite and birnessite and 0.01 M KCl for K^+-montmorillonite. Freundlich (non-linear) fits are shown for adsorption isotherms along with linear fits used for distribution coefficient calculations.

MENA showed sorptive affinity for montmorillonite, although to a lesser extent than did DNAN; MENA showed a K_d for adsorption that was ~50 % of that for DNAN in the case of Na^+-montmorillonite and 2.2 % in the case of K^+-montmorillonite. In contrast to their affinity for the silicate clays, DNAN and MENA showed little adsorption affinity for the hydroxylated surface of goethite (Figs 1, 2). Results from DNAN adsorption to birnessite also indicated near zero and negative adsorption,

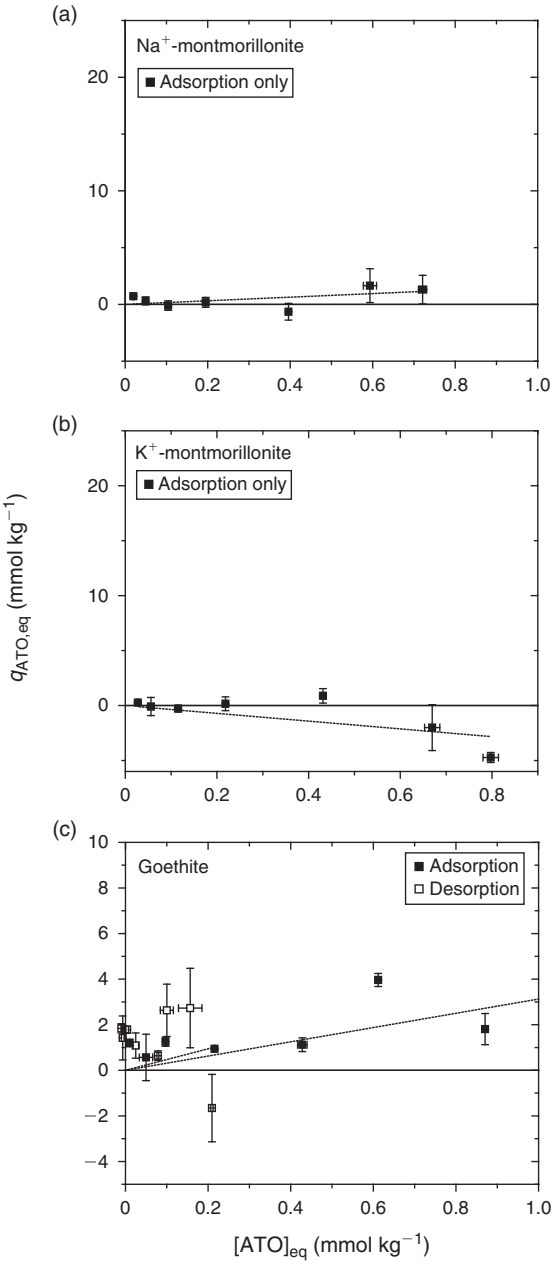

Fig. 4. Adsorption and desorption isotherms at pH 7.0 for 3-amino-1,2,4, triazole-5-one (ATO) on Na^+-montmorillonite, K^+-montmorillonite and goethite, where q represents the surface excess of adsorbate. Background electrolytes were 0.01 M NaCl for Na^+-montmorillonite, goethite and birnessite and 0.01 M KCl for K^+-montmorillonite.

consistent with interfacial exclusion (Fig. 1d). This result is in stark contrast to that of the MENA–birnessite reaction, which appears high (Fig. 2d) when calculated on the basis of loss from solution (Eqns 1, 2), which prompted the follow on mass spectrometric studies discussed in a later section.

Isotherms and mineral-surface affinities for the NHCs (NTO and ATO, Figs 3, 4) are distinctly different from those of the NACs (DNAN and MENA) presented above. When reacted with montmorillonite, the NHCs give negative or near zero surface excess values irrespective of exchangeable cation type, consistent with charge repulsion and exclusion at the clay interface (Figs 3, 4a, b). Conversely, NTO shows positive uptake to both metal oxides. NTO affinity for the goethite surface ($K_d = 11.06$, but a better fit to a Freundlich isotherm equation, Fig. 3c) greatly exceeds that of its metabolite ATO ($K_d = 3.13$, Fig. 4c). NTO exhibited its highest affinity for the birnessite surface ($K_d = 18.48$, but also a better fit to a Freundlich isotherm equation, Fig. 3d).

Repulsion of anionic NTO and ATO from the negatively charged surfaces of montmorillonite (Figs 3a, b, 4a, b) results in a negative surface excess, where analyte concentration in the bulk supernatant solution is higher than that in the entrained solution because of organic anion exclusion from the mineral–water interface.[28,29] The same effect has also been observed for other organic anions such as the glucosinolates,[30] which are naturally sulfonated organic compounds. Because of anion exclusion, the measured surface excess (q) values are shown for montmorillonite in Figs 3 and 4 only for the adsorption step. Calculation of surface excess following the desorption step leads to erroneous results as a result of a negative value for the difference within parentheses of Eqn 2. Specifically, the use of $C_{e,ads}$ overestimates, in the case of anion exclusion, adsorptive concentration in the entrained solution (M_{ENT}).

HI values calculated from the differences in slope following the adsorption and desorption steps (Figs 1–4) provide a measure of kinetic reversibility of a positive adsorption reaction. The largest HI value (least kinetically reversible reaction) was obtained for MENA reacted with K^+-montmorillonite (HI = 6.0). Several of the HI values for DNAN and MENA were in a similar range (4.3, 5.1, 6.0), in contrast to the lower HI values of NTO and ATO (1.8, 2.6, 0.5).

Oxidation of MENA and ATO by acid birnessite

Reaction of the DNAN bio-reduction product, MENA, with acid birnessite resulted in near complete removal of MENA from solution, an assessment that is apparent from the equilibrium solution phase concentrations following the adsorption step (see the x-axis scale values shown in Fig. 2d). Average removal of

Table 3. Distribution coefficients (K_d) and hysteresis indices (HI) calculated from the isotherms
DNAN, 2;4-dinitroanisole; MENA, 2-methoxy-5-nitroaniline; NTO, 3-nitro-1;2;4-triazole-5-one; ATO, 3-amino-1;2;4-triazole-5-one. NA, not applicable

Mineral sorbent	DNAN		MENA		NTO		ATO	
	Adsorption K_d	HI	Adsorption K_d	HI	Adsorption K_d	HI	Adsorption K_d	HI
Na^+-montmorillonite	29.0	4.3	16.1	3.85	−3.0[A]	0[B]	1.6	NA
K^+-montmorillonite	517	5.1	11.6	6.0	−5.3[A]	0[B]	−3.5[A]	0[B]
Goethite	−0.04[A]	0[B]	0.2	0[B]	11.1[C]	1.8	3.1	0.50
Birnessite	−0.50[A]	0[B]	5940[D]	1.2[A]	18.5[C]	2.6	ORS[D]	NA[A]

[A]Negative slopes reported as K_d.
[B]HI not calculated for negative K_d values.
[C]Better fit to Freundlich curve.
[D]ORS, oxidative removal from solution.

MENA from solution was 98.4 %. Organic degradation products were formed during MENA reaction with birnessite as evidenced by unknown (product) peak emergence during HPLC-DAD analysis. Pre- and post-reaction supernatant solutions were therefore analysed by LC-QTOF-MS in an attempt to identify the degradation products. By differential analysis, mass spectrometric peaks with *m/z* values lower (160.9860) as well as higher (174.0166, 252.9588, 335.1346) than MENA were observed. Similarly, experiments with the NTO reduction product ATO also resulted in near complete ATO removal from solution. Upon analysis with both HPLC-DAD and QTOF-MS, no ATO was detectable in the post-reaction supernatant (Fig. 5a,b).

Discussion

Adsorption trends for Na^+ and K^+ smectite

The DNAN and MENA adsorption trends for montmorillonite (Figs 1, 2) show the differential effect of exchangeable cations on NAC adsorption. Differences in affinity between Na^+ and K^+ exchanged forms of the clay suggest that the mechanisms of DNAN and MENA adsorption to montmorillonite are dominated by interaction of electronegative nitro groups on the NACs with the positively charged exchangeable cations (Na^+ or K^+). DNAN adsorption to K^+-montmorillonite was much greater than that for Na^+-montmorillonite, presumably because of the lower hydration enthalpy of K^+ (-314 kJ mol^{-1}) relative to Na^+ (-397 kJ mol^{-1}), which is known to enhance the formation of inner-sphere cation complexes with NAC nitro groups.[10]

The observed high affinity adsorption of the DNAN and MENA to the cation-saturated silicate clays is likely driven, in part, by electron donor–acceptor (EDA) complexes. An EDA complex occurs when the electron deficient π-system of the NAC, caused by the electronegative nitro-groups extracting electron density from the ring, interacts with clay surface siloxane oxygen atoms. The siloxane oxygens serve as electron donors and the π-system of the NAC as the electron acceptor, giving rise to an adsorption geometry of the ring structure that is parallel planar to the siloxane surface. This mechanism was proposed by Haderlein et al.[2] in a study where interlayer cation effects on adsorption were also examined. Consistent with the results for DNAN and MENA reported here, Haderlein et al. found that K^+-montmorillonite had the largest adsorption capacity (per unit mass) for different NACs across a range of homoionic clay minerals (montmorillonite, illite, kaolinite), and that K^+ had K_d values up to four orders of magnitude larger than other more strongly hydrated exchangeable cations (Na^+, Ca^{2+}, Mg^{2+}). Zhang et al. explored 1,3-dinitrobenzene adsorption to cation modified clays, and found again that adsorption was greatest with K^+ relative to Na^+- or Ca^{2+}-saturated smectite.[31] Boyd et al.,[10] using Fourier transform infrared (FTIR) spectroscopy to examine the adsorption mechanisms of NACs to smectite clays, showed, principally through shifts in the vibrational frequencies of the N–O bands, that adsorption was dominated by direct interaction of electronegative substituents with interlayer cations such as K^+. These authors suggested that adsorption of NACs to smectite (including montmorillonite) is likely a cumulative effect of several factors, the dominant one being the relative stability of cation–oxygen bonds formed between siloxane-adsorbed cations and nitro functional groups of the NACs.

Differences in the magnitude of DNAN and MENA adsorption to montmorillonite (Figs 1, 2) reflect the importance of nitro-cation bonding, because reduction of the *ortho*-nitro group to an amine functionality results in significantly diminished montmorillonite affinity, particularly for adsorption to the K^+-saturated clay (compare Figs 1b, 2b). For example, in the case of K^+-montmorillonite, the DNAN K_d is 517, whereas the MENA K_d is 11.6. The effect of *ortho*-nitro group reduction is much smaller, but still present, in the case of Na^+-saturation (Figs 1a, 2a), for which the DNAN $K_d = 29.04$ and the MENA $K_d = 16.05$ (Table 3). From the perspective of fate and transport of IMCs and their metabolites in soil systems, this effect is very important, because it suggests that bio-reduction of a nitro-functionality can significantly diminish contaminant sorptive affinity for layer silicate surfaces. Thus, the bio-reduced form of DNAN, expected to be formed in sub-oxic pore waters, may for this reason be more mobile in the subsurface environment. Haderlein et al.[2] argued that nitro-to-amine reduction donates electron density back to the benzene ring π-system, reducing the tendency to form an EDA complex and, hence, results in less adsorption. This EDA effect is likely superimposed on the low affinity of the $-NH_2$ group to complex even weakly hydrated cations such as K^+. The reduction of DNAN (i.e. MENA formation) leads to less adsorption because of the loss of a substituent group capable of cation complexation.

Despite these differences in magnitude, both the mono- and di-nitro aromatics showed significant adsorption to the montmorillonite surface under conditions of both K^+- and Na^+-exchangeable cation saturation, raising the question of the extent to which the IMC and its biotransformation product were adsorbed into the expansible interlayer *v.* solely on the external or basal surfaces. XRD measurements showed an increase in the d_{001} interlayer spacing (indicated by a downward shift in position 2°Θ) upon DNAN and MENA

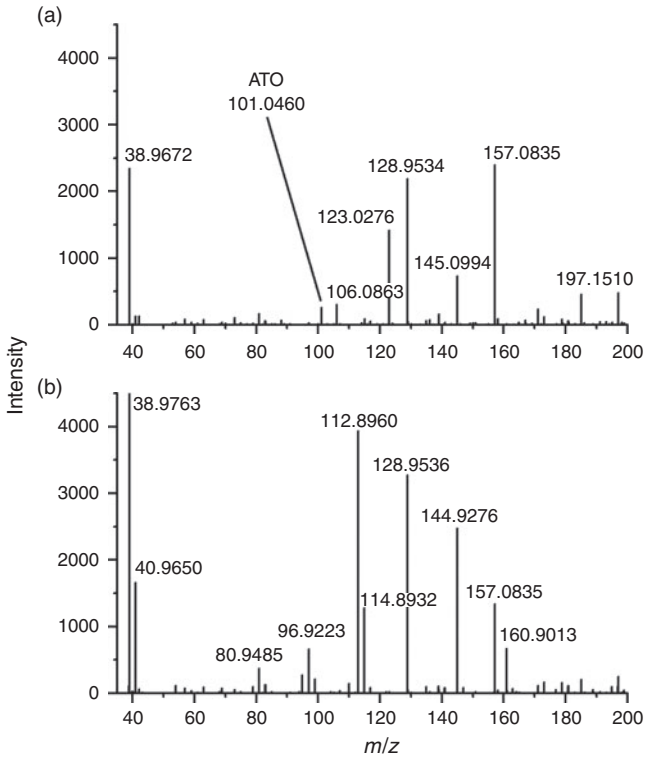

Fig. 5. Spectrometric data obtained using quadrupole time of flight mass spectrometry (QTOF-MS) in electrospray ionisation positive mode (ESI^+) for (a) the 3-amino-1,2,4,triazole-5-one (ATO) peak ($M + H^+ = 101.0460$) in stock experimental solution, and (b) following reaction with birnessite (note absence of ATO peak).

adsorption, with the largest increase observed for K^+-saturated clays (Fig. 6). This result signals interlayer (siloxane surface) adsorption of both DNAN and MENA. A model calculation also confirms that monolayer adsorption to external surfaces is insufficient to explain the moles of adsorbate of modelled molecular dimensions (Table 4), whereas co-planar orientation of the NAC adsorbate at interlayer surfaces, which is consistent with molecular modelling and prior spectroscopic studies,[10] can explain the mass balances measured in the isotherm experiments.

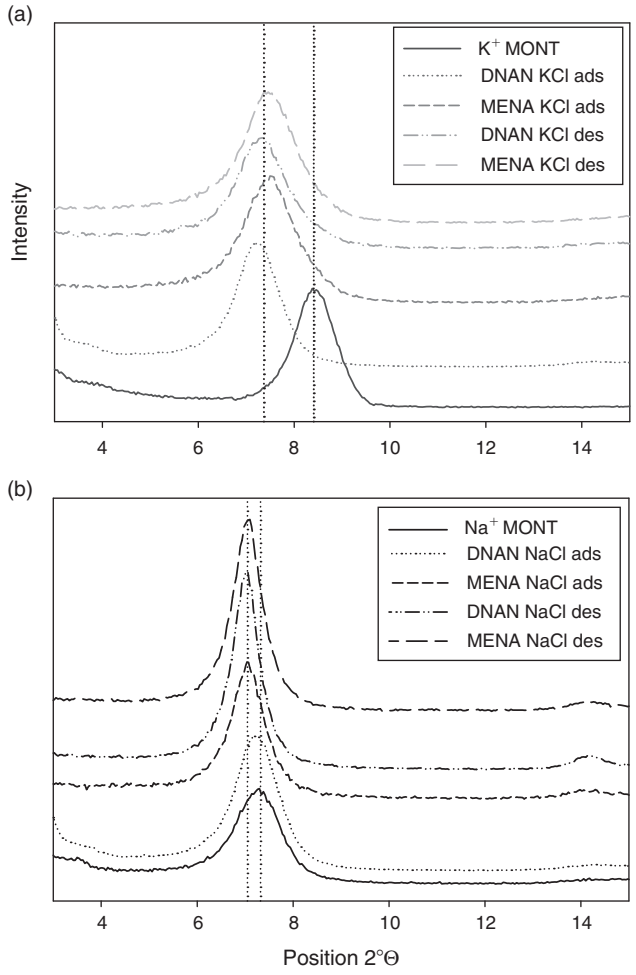

Fig. 6. X-Ray diffraction patterns for K^+-montmorillonite (MONT) (a) and Na^+-MONT (b) clays after aqueous adsorption 'ads' followed by desorption 'des' of the nitroaromatics 2,4-dinitroanisole (DNAN) and 2-methoxy-5-nitroaniline (MENA) for samples reacted at the highest adsorptive species concentrations shown in Figs 1 and 2. Note the increase in d_{001} spacing (indicated by a downward shift in position 2°Θ) with adsorption of MENA and DNAN. Greater relative expansion occurs in KCl solution and for DNAN relative to MENA, consistent with the surface excess results shown in Figs 1 and 2.

Table 4. Maximum adsorption *v.* available surface area calculations
DNAN, 2,4-dinitroanisole. DNAN surface area was determined by Connolly molecular surface area (*ChemBio 3D Ultra 13.0*)

DNAN surface area (nm^2)	DNAN adsorption (mmol kg^{-1})	Montmorillonite surface area ($m^2\ g^{-1}$)	DNAN surface density (molecules nm^{-2})	Total surface area occupied (%)
1.64	85.8	596	0.087	14
1.64	85.8	36.4	1.42	232

Specifically, the surface area of the DNAN molecule was estimated using the Connolly molecular surface area calculation in *ChemBio 3D Ultra 13.0*. Given the calculated surface area of a planar DNAN molecule as 1.64 nm^2, adsorption of the aromatic ring co-planar with the siloxane surface enables adsorption of a *maximum* of 0.61 DNAN molecules per square nanometre of planar surface (i.e. in closest-packing mode). This DNAN surface density was compared with the maximum DNAN surface excess (maximum q) measured under the following assumed scenarios: (1) DNAN adsorption to both external and interlayer surfaces and (2) DNAN adsorption only to external basal surfaces. Scenario (1) implies a DNAN surface density of ~0.09 DNAN molecules per square nanometre, or 14 % of available surfaces being occupied at maximum q. This DNAN surface density is less than the estimated maximum (0.09 DNAN molecules $nm^{-2} < 0.61$ DNAN molecules nm^{-2}) and the low surface area occupation percentage is viable, given that the isotherm is still linear at the maximum q measured. In contrast, scenario (2) implies a DNAN surface density of 1.42 DNAN molecules per nm^2, or occupation of ~232 % of the available surface sites. This cannot be reconciled with the assumption of planar adsorption to the clay mineral particles. Hence, isotherm, XRD data and model calculations are all consistent with DNAN and MENA being adsorbed to the interlayer siloxane in proportion to both their nitro functional group density and the exchangeable cation composition of the clay.

Interaction of NTO with montmorillonite resulted in negative surface excess. With a pK_a of 3.76, the NTO molecule is negatively charged at the experimental pH (pH 7). The negative charge of the sorbent evidently repels the sorptive solute, resulting in detectable levels of anion exclusion. Several authors, including, e.g. Polubesova and Borisover[32] have shown that electrostatic repulsion creates a region of anion free solution in the nanoporous domains that are present in close proximity to the solid surface. This causes an increase in adsorptive concentration in the supernatant solution relative to that measured in the bulk solution control without clay colloids (Eqn 1). An increase in exclusion (i.e. negative surface excess) with increasing equilibrium concentration in bulk solution (Fig. 2c), gives rise to the negative K_d values calculated with Eqn 3 and reported in Table 3.

Adsorption to metal oxides

NTO adsorption to the iron oxyhydroxide surface (Fig. 3c) is consistent with electrostatic considerations. In an 'indifferent' background electrolyte solution, such as the 0.01 M NaCl used here, goethite has a point of zero net charge (PZNC) of 7.5,[33] and thus is slightly positively charged at our experimental pH. This positive charge creates an electrostatic attraction between the anionic NTO and the goethite surface, giving rise to positive adsorption values. Interestingly, NTO data also suggested a high affinity for the Mn oxide, birnessite. This interaction cannot be rationalised through electrostatics alone because acid birnessite (MnO_2), has a PZNC of 1.9,[33] giving it a negative surface charge at the experimental pH. Nonetheless, we observed no new peak emergence in the HPLC-DAD chromatograms (despite extended run times) for the NTO–birnessite system, which argues against chemical transformation as a potential fate. It is plausible that NTO adsorption was localised at positively charged surface sites or mediated by cation bridging

interactions. In addition, the Freundlich isotherm equation appeared to closely approximate the adsorption of NTO to both metal oxides (Fig. 3c,d), with R^2 values of 0.97 and 0.99 for goethite and birnessite respectively.

Adsorption reversibility

Hysteresis indices were measured for all isotherms to assess the kinetic reversibility of adsorption–desorption reactions.[34] During the desorption step of the isotherm experiments, release from the surface of adsorbate occurs following perturbation by replacement of the equilibrium solution condition. When the colloidal suspensions were modified by removal of equilibrium IMC solution and replaced with an IMC-free (otherwise equivalent) electrolyte solution, the reduction in IMC concentration in solution is expected to promote IMC desorption (for positive q values) with approach to a new equilibrium value following the 3-h equilibration step (equal to that for adsorption) at a lower solution phase IMC concentration. A high HI value indicates high relative surface retention of adsorbate and, therefore, kinetic irreversibility, whereas a small or zero q value indicates adsorption–desorption that is kinetically reversible. DNAN adsorption–desorption on both the K^+- and Na^+-montmorillonite show significant hysteresis (Fig. 1a, b). The HI values are similar in scale, but HI is nonetheless 16% larger for K^+- relative to Na^+-exchanged clay. This difference in HI values is again consistent with weaker NAC ternary interaction with a strongly hydrated cation adsorbate. That is, the ternary ligand–metal–siloxane surface complexes appear to dissociate more readily for Na^+ than for K^+-exchanged forms, consistent with the lower metal–ligand stability that occurs in outer-sphere *v*. inner-sphere complexes.

For consistency across datasets, the NTO HI values were calculated using linear isotherm fits to the data shown in Fig. 3c, d for goethite and birnessite, despite the fact that isotherms were non-linear, as indicated by the non-linearity factor (n) of both Freundlich fits being <1.0. The NTO–metal oxide HI values were approximately half as large as the DNAN–clay HI values, suggesting that even though similar surface excess values are achieved in the NAC–clay and NHC–oxide systems, the electrostatic interactions leading to NHC compound adsorption (e.g. NTO to goethite) are more reversible kinetically than those for NAC–clay adsorption.

Oxidation of MENA and ATO by acid birnessite

The synthetic acid birnessite $[(Na_{0.3}Ca_{0.1}K_{0.1})(Mn^{4+}, Mn^{3+})_2O_4{\cdot}1.5H_2O]$ used in this study is a common secondary manganese oxide that is formed by bacteria and fungi in soils,[35] and it is the most commonly observed secondary Mn^{IV} solid phase. Importantly, results of our adsorption studies showed near complete removal of MENA and ATO, the bio-reduced (aminated) forms of the IMCs DNAN and NTO respectively during reaction with birnessite. Birnessite has previously been shown to remove parent aromatic amines from solution by oxidative transformation, as well as by adsorption.[18,36] Indeed, as discussed above, QToF-MS analysis indicated that birnessite induces oxidative transformation of MENA followed by potential fragment polymerisation of oxidative transformation products, an observation supported also by prior work on other aromatic amines[18] and polyphenols.[19]

ATO was also removed from solution during reaction with birnessite, and a similar oxidative transformation mechanism is hypothesised (Fig. 5). Aromatic amine transformation by Mn^{IV} oxide was investigated by Laha and Luthy,[17] who reported that azobenzene was formed from the reaction of aniline with manganese dioxide. The formation of azobenzene, a larger polymer, resulted in the removal of the NAC from solution.[17]

Conclusions

The adsorption and reactivity of IMCs with clay mineral and Fe and Mn oxide mineral constituents was determined as a means to better assess contaminant mobility and bioavailability in soils and sediments. The experimental results highlight the importance of interactions between (i) IMC chemical structure and (ii) soil mineral surface composition in controlling contaminant adsorptive affinity. Adsorption of IMCs at mineral surfaces is governed not only by functional group composition and charge of the IMCs themselves, but also by the surface functional group chemistry and (in the case of montmorillonite) exchangeable cation composition of the mineral adsorbents. For this reason, it was important to test adsorption reactions across a representative range of mineral surface chemistries characteristic of common soil mineral assemblages. While none of the minerals served as a high affinity adsorbent for all of the IMCs and metabolites studied, each of the compounds did exhibit a high adsorption affinity for at least one of the adsorbent types. This suggests that each of the compounds would be subjected to adsorptive retardation during subsurface transport, but likely as a result of accumulation at distinct mineral surfaces.

Specifically, the NACs, DNAN and MENA, exhibited significant affinity for layer silicate clays, whereas the NHCs showed greater affinity for metal oxide surfaces. NAC adsorption to layer silicate clays was apparently favoured by inner-sphere complexation between nitro functional groups and exchangeable cations, whereas NHC adsorption was insignificant on the silicate clays because of charge repulsion. Conversely, the NHC NTO exhibited strong affinity for adsorption to both goethite and birnessite surfaces.

The microbially catalysed reduction of DNAN and NTO is expected to occur in sub-oxic soil pore waters and our results indicate that such bio-reduction to MENA and ATO respectively can alter subsequent contaminant reactivity with mineral surfaces. Specifically, reduction of nitro substituents to amine functionalities diminishes NAC affinity for layer silicate surfaces, where they form ternary complexes with adsorbed metal cations. Nitro group reduction also decreases NHC sorptive affinity for goethite, but the amine functionality associated with both ATO and MENA increases their oxidative reactivity towards the mineral oxidant birnessite, supporting the assertion that a coupled biotic–abiotic degradation pathway can lead to elimination of both parent and daughter compounds.

Acknowledgements

This research was supported by the USA Department of Defence, Strategic Environmental Research and Development Program (SERDP) grant number ER2221.

References

[1] M. Smith, M. Cliff, *NTO-Based Explosives: A Technology Review* **1999** (DTSO Aeronautical Maritime Research Laboratory: Melbourne).

[2] S. B. Haderlein, K. W. Weissmahr, R. P. Schwarzenbach, Specific adsorption of nitroaromatic explosives and pesticides to clay minerals. *Environ. Sci. Technol.* **1996**, *30*, 612. doi:10.1021/ES9503701

[3] L. H. Keith, W. A. Telliard, Priority pollutants I – a perspective view. *Environ. Sci. Technol.* **1979**, *13*, 416. doi:10.1021/ES60152A601

[4] K. S. Ju, R. E. Parales, Nitroaromatic compounds, from synthesis to biodegradation. *Microbiol. Mol. Biol. Rev.* **2010**, *74*, 250. doi:10.1128/MMBR.00006-10

[5] V. Purohit, A. Basu, Mutagenicity of nitroaromatic compounds. *Chem. Res. Toxicol.* **2000**, *13*, 673. doi:10.1021/TX000002X

[6] E. L. Rylott, A. Lorenz, N. C. Bruce, Biodegradation and biotransformation of explosives. *Curr. Opin. Biotechnol.* **2011**, *22*, 434. doi:10.1016/J.COPBIO.2010.10.014

[7] V. M. Boddu, K. Abburi, S. W. Maloney, R. Damavarapu, Thermophysical properties of an insensitive munitions compound, 2, 4-dinitroanisole. *J. Chem. Eng. Data* **2008**, *53*, 1120. doi:10.1021/JE7006764

[8] C. Olivares, J. D. Liang, L. Abrell, R. Sierra-Alvarez, J. A. Field, Pathways of reductive 2,4-dinitroanisole (DNAN) biotransformation in sludge. *Biotechnol. Bioeng.* **2013**, *110*, 1595. doi:10.1002/BIT.24820

[9] L. Le Campion, A. Vandais, J. Ouazzani, Microbial remediation of NTO in aqueous industrial wastes. *FEMS Microbiol. Lett.* **1999**, *176*, 197. doi:10.1111/J.1574-6968.1999.TB13662.X

[10] S. A. Boyd, G. Y. Sheng, B. J. Teppen, C. J. Johnston, Mechanisms for the adsorption of substituted nitrobenzenes by smectite clays. *Environ. Sci. Technol.* **2001**, *35*, 4227. doi:10.1021/ES010663W

[11] C. T. Johnston, B. Khan, E. F. Barth, S. Chattopadhyay, S. A. Boyd, Nature of the interlayer environment in an organoclay optimized for the sequestration of dibenzo-*p*-dioxin. *Environ. Sci. Technol.* **2012**, *46*, 9584. doi:10.1021/ES300699Y

[12] K. W. Weissmahr, S. B. Haderlein, R. P. Schwarzenbach, R. Hany, R. Nuesch, In situ spectroscopic investigations of adsorption mechanisms of nitroaromatic compounds at clay minerals. *Environ. Sci. Technol.* **1997**, *31*, 240. doi:10.1021/ES960381+

[13] S. Chattopadhyay, S. J. Traina, Spectroscopic study of sorption of nitrogen heterocyclic compounds on phyllosilicates. *Langmuir* **1999**, *15*, 1634. doi:10.1021/LA980607H

[14] J. Chorover, M. K. Amistadi, W. D. Burgos, P. G. Hatcher, Quinoline sorption on kaolinite-humic acid complexes. *Soil Sci. Soc. Am. J.* **1999**, *63*, 850. doi:10.2136/SSSAJ1999.634850X

[15] K. Hanna, Sorption of two aromatic acids onto iron oxides: Experimental study and modeling. *J. Colloid Interface Sci.* **2007**, *309*, 419. doi:10.1016/J.JCIS.2007.01.004

[16] N. Nilsson, P. Persson, L. Lovgren, S. Sjoberg, Competitive surface complexation of o-phthalate and phosphate on goethite (α-FeOOH) particles. *Geochim. Cosmochim. Acta* **1996**, *60*, 4385. doi:10.1016/S0016-7037(96)00258-X

[17] S. Laha, R. G. Luthy, Oxidation of aniline and other primary aromatic-amines by manganese-dioxide. *Environ. Sci. Technol.* **1990**, *24*, 363. doi:10.1021/ES00073A012

[18] H. Li, L. S. Lee, D. G. Schulze, C. A. Guest, Role of soil manganese in the oxidation of aromatic amines. *Environ. Sci. Technol.* **2003**, *37*, 2686. doi:10.1021/ES0209518

[19] E. H. Majcher, J. Chorover, J. M. Bollag, P. M. Huang, Evolution of CO_2 during birnessite-induced oxidation of ^{14}C-labeled catechol. *Soil Sci. Soc. Am. J.* **2000**, *64*, 157. doi:10.2136/SSSAJ2000.641157X

[20] G. Sposito, *The Surface Chemistry of Natural Particles* **2004** (Oxford University Press: New York).

[21] R. J. Atkinson, A. M. Posner, J. P. Quirk, Adsorption of potential-determining ions at ferric oxide-aqueous electrolyte interface. *J. Phys. Chem.* **1967**, *71*, 550. doi:10.1021/J100862A014

[22] R. M. McKenzie, Synthesis of birnessite, cryptomelane, and some other oxides and hydroxides of manganese. *Mineral. Mag.* **1971**, *38*, 493. doi:10.1180/MINMAG.1971.038.296.12

[23] J. Chorover, M. K. Amistadi, Reaction of forest floor organic matter at goethite, birnessite and smectite surfaces. *Geochim. Cosmochim. Acta* **2001**, *65*, 95. doi:10.1016/S0016-7037(00)00511-1

[24] L. Le Campion, J. Ouazzani, Synthesis of 5-amino-1,2,4-triazole-3-one through the nitroreduction of 5-nitro-1,2,4-triazole-3-one. Comparison between chemical and microbiological catalysis. *Biocatalysis Biotransform.* **1999**, *17*, 37. doi:10.3109/10242429909003205

[25] L. Le Campion, C. Giannotti, J. Ouazzani, Photocatalytic degradation of 5-nitro-1,2,4-triazol-3-one NTO in aqueous suspension of TiO_2. Comparison with Fenton oxidation. *Chemosphere* **1999**, *38*, 1561. doi:10.1016/S0045-6535(98)00376-2

[26] B. Rao, W. Wang, Q. S. Cai, T. Anderson, B. H. Gu, Photochemical transformation of the insensitive munitions compound 2,4-dinitroanisole. *Sci. Total Environ.* **2013**, *443*, 692. doi:10.1016/J.SCITOTENV.2012.11.033

[27] W. L. Huang, H. Yu, W. J. Weber, Hysteresis in the sorption and desorption of hydrophobic organic contaminants by soils and sediments – 1. A comparative analysis of experimental protocols. *J. Contam. Hydrol.* **1998**, *31*, 129. doi:10.1016/S0169-7722(97)00056-9

[28] J. Jerez, M. Flury, Humic acid-, ferrihydrite-, and aluminosilicate-coated sands for column transport experiments. *Colloid Surf. A* **2006**, *273*, 90. doi:10.1016/J.COLSURFA.2005.08.008

[29] C. Tournassat, C. A. J. Appelo, Modelling approaches for anion-exclusion in compacted Na-bentonite. *Geochim. Cosmochim. Acta* **2011**, *75*, 3698. doi:10.1016/J.GCA.2011.04.001

[30] A. L. Gimsing, J. C. Sorensen, B. W. Strobel, H. C. B. Hansen, Adsorption of glucosinolates to metal oxides, clay minerals and humic acid. *Appl. Clay Sci.* **2007**, *35*, 212. doi:10.1016/J.CLAY.2006.08.008

[31] L. C. Zhang, L. Luo, S. Z. Zhang, Adsorption of phenanthrene and 1,3-dinitrobenzene on cation-modified clay minerals. *Colloids Surf. A Physicochem. Eng. Asp.* **2011**, *377*, 278. doi:10.1016/J.COLSURFA.2011.01.017

[32] T. Polubesova, M. Borisover, Two components of chloride anion exclusion volume in montmorillonitic soils. *Colloids Surf. A Physicochem. Eng. Asp.* **2009**, *347*, 175. doi:10.1016/J.COLSURFA.2009.04.002

[33] J. Chorover, Zero-charge points, in *Encyclopedia of Soils in the Environment* (Ed. D. L. Sparks) **2005**, pp. 367–373 (Elsevier: Oxford, UK).

[34] J. Chorover, M. L. Brusseau, Kinetics of sorption–desorption, in *Kinetics of Water–Rock Interaction* (Ed S. L. Brantley, J. D. Kubicki, A. F. White). **2008**, pp. 109–149 (Springer: New York).

[35] B. M. Tebo, J. R. Bargar, B. G. Clement, G. J. Dick, K. J. Murray, D. Parker, R. Verity, S. M. Webb, Biogenic manganese oxides: properties and mechanisms of formation. *Annu. Rev. Earth Planet. Sci.* **2004**, *32*, 287. doi:10.1146/ANNUREV.EARTH.32.101802.120213

[36] Y. He, J. Xu, Y. Zhang, C. S. Guo, L. Li, Y. Q. Wang, Oxidative transformation of carbamazepine by manganese oxides. *Environ. Sci. Pollut. Res. Int.* **2012**, *19*, 4206. doi:10.1007/S11356-012-0949-2

[37] C. O. Ijagbemi, M. Baek, D. Kim, Montmorillonite surface properties and sorption characteristics for heavy metal removal from aqueous solutions. *J. Hazard. Mater.* **2009**, *166*, 538. doi:10.1016/J.JHAZMAT.2008.11.085

[38] *5-Nitro-o-anisidine (CAS 99-59-2)* **2007**. Available at http://toxnet.nlm.nih.gov/cpdb/chempages/5-NITRO-o-ANISIDINE.html [Verified 8 December 2014].

[39] N. Bhatnagar, G. Kamath, J. J. Potoff, Prediction of 1-octanol-water and air-water partition coefficients for nitro-aromatic compounds from molecular dynamics simulations. *Phys. Chem. Chem. Phys.* **2013**, *15*, 6467. doi:10.1039/C3CP44284E

[40] K.-Y. Lee, L. B. Chapman, M. D. Cobura, 3-Nitro-1,2,4-triazol-5-one, a less sensitive explosive. *J. Energ. Mater.* **1987**, *5*, 27. doi:10.1080/07370658708012347